CHANNEL ADAPTIVE PULSE SHAPING FOR OQAM-OFDM SYSTEMS

Martin Fuhrwerk and Jürgen Peissig

Institute of Communication Technologies
Leibniz Universität Hannover
{fuhrwerk,peissig}@ikt.uni-hannover.de

Malte Schellmann

Huawei European Research Center
Munich
malte.schellmann@huawei.com

ABSTRACT

Theory predicts a gain in transmission performance, when adapting pulse shapes of Offset Quadrature Amplitude Modulation (OQAM) Orthogonal Frequency Division Multiplexing (OFDM) systems to delay and Doppler spread in doubly-dispersive channels. Here we investigate the quantitative gains in reconstruction quality and bit error rate (BER) with respect to subcarrier spacing and channel properties. It is shown that it is possible to reduce the uncoded BER by a factor of more than two and the coded BER by a factor of at least four, utilizing only two different pulse shapes. The simulation results show that channel adaptive pulse shaping for OQAM-OFDM systems is a promising concept for future mobile communication systems.

Index Terms— OQAM-OFDM, Pulse shaping, Prototype filter, FBMC

1. INTRODUCTION

An ever growing demand for high data rates with the ubiquitous need for mobility drives recent wireless communication systems to deliver adequate solutions. The application of multiple antenna scheme technologies as well as establishing an increased cell density and efficient utilization of available time and frequency resources can provide a significant contribution towards a more efficient utilization of spectrum. Currently deployed multi-carrier systems based on Cyclic-Prefix OFDM (CP-OFDM), e.g. LTE, DVB-T or WiFi, suffer from high out-of-band emissions due to the inherent rectangular pulse shaping. This increases the need for guard bands for interference protection leading to an under-utilization of the spectrum. One approach to enhance spectral efficiency is to utilize OQAM-OFDM with flexible pulse shaping based on Filter Bank Multi-Carrier (FBMC). OQAM-OFDM allows to use arbitrary pulse shapes in contrast to CP-OFDM, enabling to reduce side lobes and thus improves the coexistence capabilities of a communication system with adjacent or in-band interferer [1] and is more robust to inter carrier interference (ICI). However, OQAM-OFDM systems are more vulnerable to intersymbol interference (ISI) due to the absence of a cyclic prefix.

A theoretical analysis of the impact of doubly-dispersive channels on the performance of FBMC systems has been made in [2] by Strohmer and Beaver. They obtain the optimal lattice grid structure and pulse shape for certain channel environments. Another approach to minimize the impact of doubly-dispersive channels on FBMC systems has been presented in [3]. Here a transmission scheme based on Gaussian pulse shape and adaptive lattice grid density is presented. In [4] the performance of the Isotropic Orthogonal Transform Algorithm (IOTA) based on extended Gaussian functions (EGF) for selected time and time-frequency dispersive channels is compared to CP-OFDM. It is shown that pulse shape adaptation with respect to channel state information can actually improve the system performance.

In this work we investigate the quantitative gains achievable by channel adaptive pulse shape selection for FBMC systems. Therefore we consider several pulse shapes from literature suggested for OQAM-OFDM and assume its fixed lattice grid for a reduced parameter set and signaling overhead. The influence of doubly-dispersive channels on the intrinsic interference of FBMC systems is studied in terms of reconstruction quality and bit error rate with respect to channel properties and subcarrier spacing.

The rest of the paper is organized as follows. In section 2 the OQAM-OFDM system model and its intrinsic interference are described, followed by an overview on the applied prototype filter functions in section 3. The simulation results are discussed in section 4 and finally summarized in the conclusion.

2. SYSTEM MODEL

In this section, we first provide a description of the system model applied in this paper. Second the metric for evaluation of the reconstruction performance in doubly-dispersive channels is derived. As this work merely focuses on the influence of the intrinsic interference of OQAM-OFDM systems, the noise is neglected in our investigation. Therefore, the general time-discrete system model considered in this paper can be described by

$$r(n) = \sum_{\tau} h(n,\tau)s(n-\tau), \tag{1}$$

whereby the received signal $r(n)$ at sample index n is an aggregation of the transmit signal $s(n)$, passing through the time-variant mobile communication channel $h(n,\tau)$. τ refers to the channel tap indices normalized to the sampling period.

For an OQAM-OFDM system, the critically sampled transmit signal $s(n)$ is given by

$$s(n) = \sum_{m=-\infty}^{\infty} \sum_{k=-\frac{K}{2}}^{\frac{K}{2}-1} j^{m+k} d_{k,m} p_k\left(n - m\tau_0 K\right) \tag{2}$$

where $d_{k,m}$ is a real valued OQAM symbol mapped to subcarrier k at the m-th FBMC symbol. K indicates the number of total subcarriers and $p_k(n)$ is the real valued and symmetric pulse shape $p(n) = p^*(-n)$ modulated to subcarrier k given by

$$p_k(n) = p(n) e^{-j2\pi\nu_0 k \frac{n}{K}}. \tag{3}$$

Here, τ_0 and ν_0 are the normalized symbol and subcarrier spacing, respectively. These parameters specify the applied lattice grid relative to the symbol duration and are set to $\tau_0 = 0.5$ and $\nu_0 = 1$ for OQAM-OFDM, so that $\tau_0\nu_0 = 0.5$ holds. Under the mandatory condition for the pulse shape $p^*(-n) = p(n)$ met for OQAM-OFDM, the received real OQAM symbols $\tilde{d}_{\tilde{k},\tilde{m}}$ can be detected utilizing the matched filter as below:

$$\tilde{d}_{\tilde{k},\tilde{m}} = \Re\left\{ j^{-(\tilde{m}+\tilde{k})} \sum_{n=-\infty}^{\infty} r(n) p_{\tilde{k}}^*\left(n - \tilde{m}\tau_0 K\right) \right\}. \tag{4}$$

For channel free transmission, i.e. $r(n) = s(n)$, and by application of the ambiguity function $A(\tau,\nu)$ for real valued pulse shapes

$$A(\tau,\nu) = \sum_{n=-\infty}^{\infty} p(n) p^*(n-\tau K) e^{-j2\pi\nu\frac{n}{K}}; \tau K \in \mathbb{Z}, \nu \in \mathbb{R}, \tag{5}$$

(4) can be split into a data and an interference part according to

$$\begin{aligned}
\tilde{d}_{\tilde{k},\tilde{m}} &= \Re\left\{ j^{-(\tilde{m}+\tilde{k})} \sum_{n=-\infty}^{\infty} s(n) p_{\tilde{k}}^*\left(n - \tilde{m}\tau_0 K\right) \right\} \\
&= \Re\Bigg\{ \sum_{m=-\infty}^{\infty} \sum_{k=-\frac{K}{2}}^{\frac{K}{2}-1} j^{-(\tilde{m}+\tilde{k})} j^{m+k} d_{k,m} \\
&\quad \cdot \underbrace{\sum_{n=-\infty}^{\infty} p_k\left(n - m\tau_0 K\right) p_{\tilde{k}}^*\left(n - \tilde{m}\tau_0 K\right)}_{A\left((\tilde{m}-m)\tau_0,(\tilde{k}-k)\nu_0\right)} \Bigg\} \\
&= \underbrace{d_{\tilde{k},\tilde{m}} \Re\{A(0,0)\}}_{\text{data}} \\
&\quad + \underbrace{\sum_{\mu} \sum_{\substack{\kappa \\ |\mu|+|\kappa|\neq 0}} d_{\tilde{k}-\kappa,\tilde{m}-\mu} \Re\left\{ j^{-(\kappa+\mu)} A(\mu\tau_0, \kappa\nu_0) \right\}}_{\text{intrinsic interference}},
\end{aligned} \tag{6}$$

where $\mu = \tilde{m} - m$ and $\kappa = \tilde{k} - k$ are the difference between the OQAM symbols and subcarriers, respectively.

To measure the reconstruction performance the signal-to-interference ratio (SIR) is used, which determines the amount of intrinsic interference power σ_I^2, also known as orthogonality parameter [4], induced to the demodulated data of $\tilde{d}_{\tilde{k},\tilde{m}}$ of power σ_s^2. It is defined according to

$$SIR = \frac{\sigma_s^2}{\sigma_I^2} = \frac{\sigma_s^2}{\sum\limits_{\mu} \sum\limits_{\substack{\kappa \\ |\mu|+|\kappa|\neq 0}} \sigma_I^2(\mu,\kappa)}, \tag{7}$$

whereby $\sigma_I^2(\mu,\kappa)$ is the intrinsic interference power inflicted by the OQAM symbol with symbol and subcarrier offset μ and κ, respectively, see (6). Assuming $\mathbb{E}\{|d_{k,m}|^2\} = 1/2$, the average energy $\sigma^2 = \mathbb{E}\{|\tilde{d}_{\tilde{k},\tilde{m}}|^2\}$ received per OQAM symbol can be obtained from (6) according to

$$\begin{aligned}
\sigma^2 &= \underbrace{\frac{1}{2}|\Re\{A(0,0)\}|^2}_{\sigma_s^2} \\
&\quad + \sum_{\mu} \sum_{\substack{\kappa \\ |\mu|+|\kappa|\neq 0}} \underbrace{\frac{1}{2}|\Re\{j^{-(\mu+\kappa)} A(\mu\tau_0, \kappa\nu_0)\}|^2}_{\sigma_I^2(\mu,\kappa)}.
\end{aligned} \tag{8}$$

Now we consider the influence of time-variant channels $h(n,\tau)$. For channels satisfying the WSSUS condition [5], the SIR is given by

$$SIR = \frac{\sigma_{s,h}^2}{\sum\limits_{\mu} \sum\limits_{\substack{\kappa \\ |\mu|+|\kappa|\neq 0}} \sigma_{I,h}^2(\mu,\kappa)}, \tag{9}$$

where $\sigma_{s,h}^2$ and $\sigma_{I,h}^2$ are the channel depended data and interference powers, respectively. As derived in [5], $\sigma_{s,h}^2$ and $\sigma_{I,h}^2$ can be calculated by a two-dimensional convolution of the related ambiguity function and the channel scattering function $S_h(\tau,\nu)$ according to

$$\sigma_{s,h}^2 = \sum_{\tau} \sum_{\nu} S_h(\tau,\nu) |\Re\{A(\tau,\nu)\}|^2 \tag{10}$$

$$\begin{aligned}
\sigma_{I,h}^2(\mu,\kappa) &= \sum_{\tau} \sum_{\nu} S_h(\tau,\nu) \\
&\quad \cdot |\Re\{j^{-(\mu+\kappa)} A(\mu\tau_0 + \tau, \kappa\nu_0 + \nu)\}|^2.
\end{aligned} \tag{11}$$

Note that $S_h(\tau,\nu)$ is the real-valued product of the Doppler power spectral density and the power delay profile of the applied channel.

3. PULSE SHAPE DESCRIPTION

The pulse shapes considered in this work are derived from truncated prototype filter functions according to

$$p(n) = \begin{cases} p_p(n), & |n| < \frac{\gamma K}{2} \\ 0, & \text{otherwise} \end{cases}, \tag{12}$$

where $p_p(n)$ describes the time-unlimited pulse shape. Here, γ is the overlapping factor so that the used pulse shape with odd symmetry amounts to a length of $L = \gamma K - 1$ samples.

3.1. Phydyas Pulse Shape

The pulse shape, which has been presented first in [6] and intensively studied within the PHYDYAS project, is a time limited Nyquist filter obtained by frequency sampling and optimized to have a superior stop band attenuation. Due to this property, the Phydyas pulse shape is a good choice for spectrum sharing scenarios. The prototype filter function $p_p(n)$ can be described by a truncated Fourier series with coefficients a_l according to [6]

$$p_p(n) = a_0 + 2\sum_{l=1}^{\gamma-1} a_l \cos\left(\frac{2\pi l n}{\gamma K}\right). \tag{13}$$

3.2. IOTA Pulse Shape / EGF

The Gaussian prototype filter has ideal energy localization in the time-frequency grid, but does not satisfy the Nyquist criteria. Therefore, the Isotropic Orthogonal Transform Algorithm (IOTA) is used to transform the non-orthogonal Gaussian function into a prototype filter function which is orthogonal after matched filtering at the receiver side. Thereby the localization property of the Gaussian function is kept. In this paper we use the closed form solution based on extended Gaussian functions (EGF) reported in [7], which can be written as

$$p_p(n,\alpha) = \frac{1}{2}\sum_{k=0}^{\infty} a_{k,\alpha,\nu_0}\left[g_\alpha\left(\frac{n}{K}+\frac{k}{\nu_0}\right)+g_\alpha\left(\frac{n}{K}-\frac{k}{\nu_0}\right)\right] \cdot \sum_{l=0}^{\infty} a_{l,1/\alpha,\tau_0}\cos\left(2\pi l\frac{n}{\tau_0 K}\right). \tag{14}$$

Here α is the spreading factor of the applied Gaussian function g_α used to adapt the power spreading in the time-frequency grid and $a_{\{\cdot\}}$ are real valued weighting coefficients given in [7].

3.3. Hermite Pulse Shape

Similar to the IOTA pulse shape the Hermite prototype filter is derived from the Gaussian function. Simulations have shown, that it provides a better localization property compared to the IOTA pulse shape, in case both prototype filter functions are truncated to length L. For the Hermite pulse shape the Gaussian function is weighted with isotropic Hermite functions to achieve orthogonality [8]. The Hermite pulse shape is build according to

$$p_p(n) = \sum_{k=0}^{N_H-1} a_{4k} H_{4k}\left(2\sqrt{\pi}\frac{n}{K}\right) \tag{15}$$

$$\text{with } H_l(n) = e^{-\frac{n^2}{2}}\frac{d^l}{dn^l}e^{-n^2},$$

where a_{4k} represent the weighting coefficients reported in [8], $\frac{d^l}{dn^l}$ being the l-th derivation with respect to n and $N_H = 4$ is the number of the first isotropic Hermite functions.

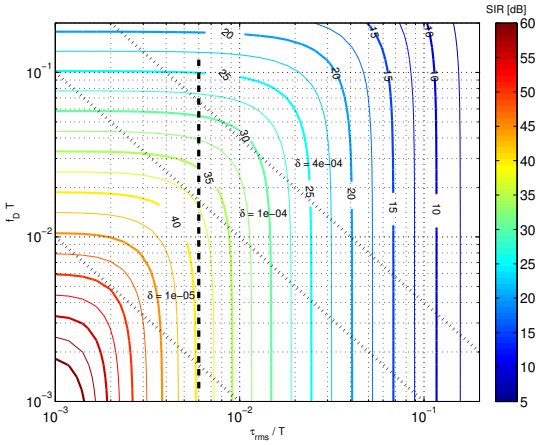

Fig. 1: SIR of the IOTA/EGF with $\alpha = 3$ in dependence of normalized delay spread τ_{rms}/T and Doppler shift $f_D T$. The dashed diagonals indicate the SIR which is available in a certain channel scenario by changing the symbol duration T and subcarrier spacing Δf, respectively.

4. SIMULATION RESULTS

First, we investigate the pulse shape dependent SIR in doubly-dispersive channel environments. Second an analysis of the overall system performance in terms of bit error rate for a specific channel setup is provided. All evaluations are performed with $K = 128$ and $\gamma = 4$ to provide a good compromise between system complexity and filter truncation effects. Furthermore, we assume perfect time and frequency synchronization as well as perfect channel knowledge at receiver side. In this study a Rayleigh fading channel with an exponential decay power delay profile and Jakes' Doppler power spectrum is considered. The related channel scattering function is given by

$$S_h(\tau,\nu) = \frac{e^{-\frac{\tau}{K\check{\tau}_{rms}}}}{\check{\tau}_{rms}} \frac{1}{\pi\check{f}_D\sqrt{1-\left(\frac{\nu}{K\check{f}_D}\right)^2}}, \tag{16}$$

whereby $\check{\tau}_{rms}$ and $\check{f}_D$ denote the delay spread and the maximum Doppler shift normalized to the symbol duration and the subcarrier spacing, respectively.

4.1. Reconstruction performance

The SIR is evaluated according to (9) with the channel scattering function (16). An example of the SIR of an IOTA/EGF pulse shape with $\alpha = 3$ is illustrated in Fig. 1. The figure shows how to choose the symbol duration T for an OQAM-OFDM system to maximize the SIR under a certain channel environment.

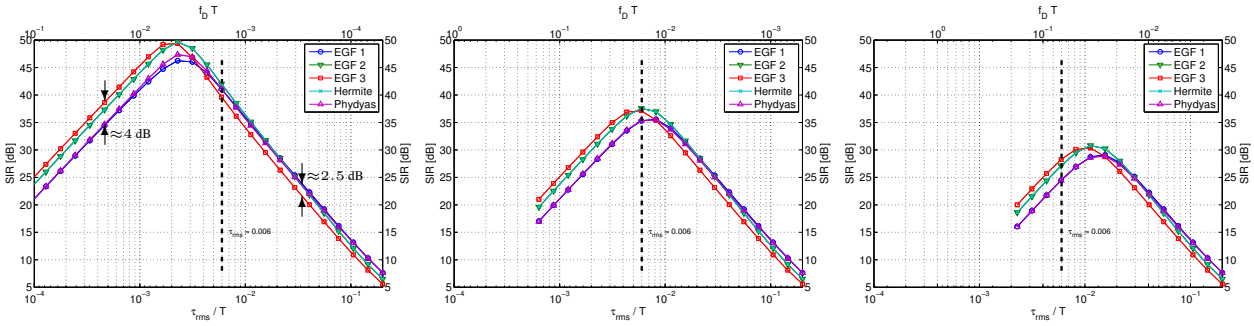

(a) $\delta = 10^{-5}$ (v = 5km/h) (b) $\delta = 10^{-4}$ (v = 50km/h) (c) $\delta = 4 \cdot 10^{-4}$ (v = 200km/h)

Fig. 2: Reconstruction performance (SIR) of IOTA/EGF with $\alpha = \{1, 2, 3\}$, Hermite and Phydyas pulse shapes for different channel conditions δ (ref. Fig. 1) at different velocities

Channel scenario	f_c	1.8 GHz
	τ_{rms}	1.2 μs
	v	[5, 50, 200] km/h
System parameters	K	128
	γ	4
	T, Δf	200 μs, 5 kHz
Effective channel parameters	τ_{rms}/T	$6 \cdot 10^{-3}$
	$f_D T$	$[(5/3, 50/3, 200/3) \cdot 10^{-3}]$
	f_D	$\approx$ [8, 83, 3333] Hz

Table 1: Parameter setup for the performance evaluation of pulse shapes in different channel environments. The Doppler frequencies represent pedestrians, urban traffic and high speed.

Assuming the symbol duration T being a free system design parameter, modifying T will change $\check{\tau}_{rms}$ and $\check{f}_D$ but not the channel characteristics. Therefore we define the Delay-Doppler-Spread δ as channel characteristic used in our investigation according to

$$\delta = \check{\tau}_{rms} \check{f}_D = \tau_{rms} f_D. \tag{17}$$

Therefore $\check{f}_D = \delta / \check{\tau}_{rms}$ defines the section line in the two-dimensional SIR space available for a specific system in a certain channel. For the channel scenario given in Table 1, the related Delay-Doppler Spread curves are shown in dotted lines in Fig. 1 and depicted distinctively in Fig. 2. Depending on the channel environment δ, the gain from switching pulse shapes exceeds more than 4 dB for Doppler spread dominated channels and approximately 2.5 dB for delay spread dominated ones. These differences in gain, when comparing the two extremes, can be explained by filter truncation effects, as time-domain filter truncation induces a power spread to the side lobes in frequency domain which increases the vulnerability to Doppler spreads.
Considering an environment with a certain delay spread but different Doppler spreads as defined in Table 1, a system design with a fixed pulse shape for all scenarios would lead to

Modulation	16-QAM
Equalizer	One-Tap Zero-Forcing
Encoder	Convolutional ([171, 133])
Code rate	2/3
Decoder	Hard-bit Viterbi
# of symbols per frame	1000
# of channels per sim	500

Table 2: Simulation setup for the BER performance evaluation of pulse shapes.

significant performance losses in at least one of these scenarios. For the urban traffic scenario ($\delta = 10^{-4}$) as depicted in Fig. 2b and for $\tau_{rms}/T = 6 \cdot 10^{-3}$, changing pulse shapes would provide only slight gains in SIR, but an OQAM-OFDM system can gain either about 2.5 dB in pedestrian environments (Fig. 2a) or more than 4 dB in high speed environments (Fig. 2c), in case a change of the applied pulse shape is allowed. According to the direction parameter and Heisenberg uncertainty, Hermite pulse shape and IOTA with $\alpha = 2$ have approximately the same SIR, which was in good agreement with our investigations. Therefore, IOTA with $\alpha = 2$ is not considered in the rest of the investigations.

4.2. System performance

For the BER analysis, we used Monte-Carlo simulations of a polyphase network based FBMC implementation with the parameter setup given in Table 2, frame-wide interleaving and perfect synchronization and channel knowledge. Fig. 3 and 4 depict the uncoded and coded BER, respectively. By a proper pulse shape selection the uncoded BER can be improved by a factor of at least two (Fig. 3). By choosing a suitable channel coding and code rate (Fig. 4), the BER can be decreased by a factor of more than four in high mobility environments. These gains can be achieved by utilizing only two different pulse shapes, namely a IOTA/EGF pulse shape with $\alpha = 3$ for Doppler spread and the Phydyas pulse shape for delay spread dominated channels, respectively.

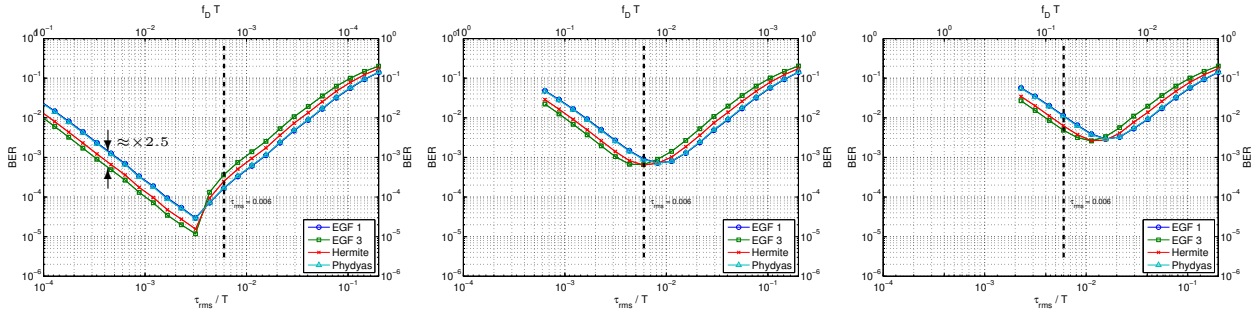

(a) $\delta = 10^{-5}$ ($v = 5$km/h) (b) $\delta = 10^{-4}$ ($v = 50$km/h) (c) $\delta = 4 \cdot 10^{-4}$ ($v = 200$km/h)

Fig. 3: Uncoded BER for a 16-QAM in different channel conditions at different velocities

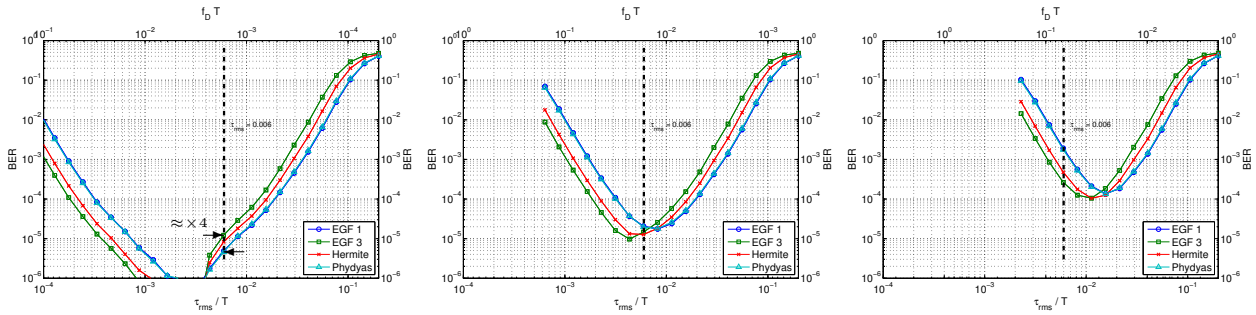

(a) $\delta = 10^{-5}$ ($v = 5$km/h) (b) $\delta = 10^{-4}$ ($v = 50$km/h) (c) $\delta = 4 \cdot 10^{-4}$ ($v = 200$km/h)

Fig. 4: BER for a 16-QAM in different channel conditions at different velocities with convolutional code of rate $2/3$

Additionally, all BER curves show the same trend as the corresponding SIR plots. Therefore SIR can be suggested to be a useful tool for the performance evaluation of pulse shapes in doubly-dispersive channels.

5. CONCLUSION

We quantitatively assessed the gain achievable from adapting the pulse shape to doubly-dispersive channels, which is suggested from theory [2]. The evaluation results show that by utilizing only two different pulse shapes, the coded BER can be reduced by a factor of more than four and the uncoded BER by a factor of at least two. Additionally it is shown that the SIR can be suggested to be a useful tool for the performance evaluation of pulse shapes in doubly-dispersive channels.

REFERENCES

[1] Ari Viholainen, Maurice Bellanger, and Mathieu Huchard, "Prototype filter and structure optimization," Tech. Rep., www.ict-phydyas.org, 2009.

[2] Thomas Strohmer and Scott Beaver, "Optimal ofdm design for time-frequency dispersive channels," *IEEE Transactions on Communications*, vol. 51, no. 7, pp. 1111–1122, July 2003.

[3] F.M. Han and X.D. Zhang, "Wireless multicarrier digital transmission via weyl-heisenberg frames over time-frequency dispersive channels," *IEEE Transactions on Communications*, vol. 57, no. 6, pp. 1721–1733, June 2009.

[4] Jinfeng Du and Svante Signell, "Pulse shape adaptivity in OFDM/OQAM systems," in *Proceedings of the 2008 International Conference on Advanced Infocomm Technology - ICAIT '08*, New York, New York, USA, 2008, pp. 1–5, ACM Press.

[5] J. Du and S. Signell, "Novel Preamble-Based Channel Estimation for OFDM/OQAM Systems," *2009 IEEE International Conference on Communications*, pp. 1–6, June 2009.

[6] Shahriar Mirabbasi and Ken Martin, "Design of prototype filter for near-perfect-reconstruction overlapped complex-modulated transmultiplexers," in *2002 IEEE International Symposium on Circuits and Systems. Proceedings (Cat. No.02CH37353)*. vol. 1, pp. I–821–I–824, IEEE.

[7] Pierre Siohan and Christian Roche, "Cosine-modulated filterbanks based on extended Gaussian functions," *IEEE Transactions on Signal Processing*, vol. 48, no. 11, pp. 3052–3061, 2000.

[8] R. Haas and J.-C. Belfiore, "Multiple carrier transmission with time-frequency well-localized impulses," in *IEEE Second Symposium on Communications and Vehicular Technology in the Benelux*. 1994, number 2, pp. 187–193, Univ. Catholique de Louvain.